THE JOURNAL OF PHYSICAL CHEMISTRY Letters

Letter

pubs.acs.org/JPCL

How Inter- and Intramolecular Processes Dictate Aggregation-Induced Emission in Crystals Undergoing Excited-State Proton Transfer

Michael Dommett, Miguel Rivera, and Rachel Crespo-Otero*

School of Biological and Chemical Sciences, Materials Research Institute, Queen Mary University of London, Mile End Road, London E1 4NS, United Kingdom

Supporting Information

ABSTRACT: Aggregation-induced emission (AIE) offers a route for the development of luminescent technologies with high quantum efficiencies. Excited-state intramolecular proton transfer (ESIPT) coupled to AIE can produce devices with emission across the visible spectrum. We use a combination of theoretical models to determine the factors that mediate fluorescence in molecular crystals undergoing ESIPT. Using two materials based on 2′-hydroxychalcone as exemplar cases, we analyze how inter- and intramolecular processes determine the emissive properties in the crystal environment. This systematic investigation extends the current interpretation of AIE to polar chromophores with multiple decay pathways. We find that population of nonradiative pathways is dictated by the electronic effects of the substituents and the degree of distortion allowed in the crystal environment. Localization of the electron density is crucial to maximize fluorescence via ESIPT. Our conclusions offer design strategies for the development of luminescent molecular crystals.

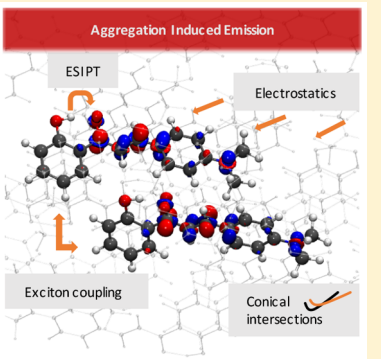

A major obstacle in the fabrication of highly emissive devices such as organic lasers is aggregation-caused quenching (ACQ), a common phenomenon where highly fluorescent compounds in aqueous phase become dark in the solid state. Contrastingly, aggregation-induced emission (AIE) occurs when nonemissive chromophores in dilute solution become luminescent upon aggregation.

AIE offers a route for the manufacture of organic optoelectronic devices, where highly efficient and tunable luminescence in the solid state is required for optimum performance.[1−3] Proposed AIE mechanisms include J-aggregate formation, excimer emission, restriction of intramolecular motions (RIM), restricted access to the conical intersection (RACI), cis−trans isomerization, and clusteroluminescence.[1−13]

AIE has commonly been understood through the RIM model, where low-frequency rotational modes of phenyl rings dissipate energy nonradiatively in solution.[1−3] In the solid state, the nonradiative decay channel is suppressed, increasing the quantum yield of fluorescence. Results from the RIM model, while extremely informative, are based on the vibronic coupling scheme assuming harmonic behavior, while low-frequency modes can be highly anharmonic.[14−16]

As an alternative approach, the RACI model proposed by Blancafort et al. directly considers the role of the S_1−S_0 conical intersections (CIs), which in the solid state lie higher in energy due to environmental hindrance.[7,8] RIM and RACI models have been used in combination with QM/MM methods to consider slightly polar systems.[17−26] One yet unexplored question is how intermolecular and intramolecular factors can be used to tune the underlying nonradiative mechanisms.

Excited-state intramolecular proton transfer (ESIPT) systems displaying AIE have been used in laser dyes, molecular probes, and optoelectronics, where the large Stokes-shifted emission prevents self-absorption and increases efficiency.[27−30] An intramolecular hydrogen bond mediates tautomerization between enol (E) and keto (K) forms in a fully reversible four-level photocycle (E → E* → K* → K). Fluorescence can occur from either or both of the E*/K* states, the ratio of which is influenced by factors such as substituents, solvent polarity, and viscosity.[18,31−40] Because of the polarity of the molecules involved, the presence of multiple decay channels, and the role of the environment, ESIPT crystals represent ideal candidates to study the interplay between inter- and intramolecular factors in AIE chromophores.

We investigate the differing AIE behavior of two crystals based on 2′-hydroxychalcone (Figure 1). Pertinently, the identity of substituents on the 2′-hydroxychalcone skeleton determines the crystalline structure and the quantum yield of fluorescence.[41] Compound **1** exhibits AIE and has promising properties for solid state lasers. In contrast, compound **2** is dark in both solution and the solid state.

In **1**, chromophores aggregate in a slip-stacking, herringbone structure in an edge to face arrangement (Figure 1). Conversely, in **2** the dominant motif is the face-to-face π−π

Received: October 31, 2017
Accepted: December 8, 2017
Published: December 8, 2017

DOI: 10.1021/acs.jpclett.7b02893
J. Phys. Chem. Lett. XXXX, XXX, XXX−XXX

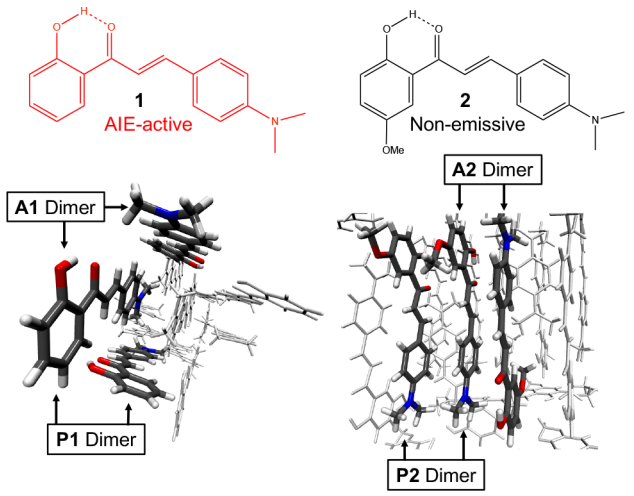

Figure 1. Molecular and crystal structures of the two compounds under investigation. Compound **1**, left, displays AIE behavior, whereas **2**, right, is nonemissive in both aqueous and solid phases. Also labeled are the parallel (**P**) and antiparallel (**A**) dimer configurations.

stacking of chromophores. For both crystals, two dimer configurations are present, where monomers are arranged parallel (**P**) and antiparallel (**A**) (Figure 1). Both arrangements were considered in our calculations.

To provide a complete picture of the factors affecting decay mechanisms in these materials, we use a combination of solid-state and excited-state embedding calculations. First, we optimized the experimental crystal structures of **1** and **2** with PBE-D2 using Quantum Espresso.[41,42] Excited-state calculations were simulated using TDDFT with electrostatic and mechanical embedding applying the ONIOM-(TDDFT):AMBER method.[43−45] The ωB97x-D functional was used with the 6-31G(d) and 6-311++G(d,p) basis sets. Additionally, RI-CC2/def2-TZVP-embedded calculations were performed. S_1−S_0 minimal energy conical intersection (MECI) geometries of **1** and **2** in both vacuum and the solid state were obtained with SA-2-CASSCF(12,11)/6-31G(d) and QM/MM (AMBER force field). In the case of TDDFT, a modified version of the CIOpt program was applied to locate S_1−S_0 MECIs.[46,47]

The nature of the crystal packing and the polarity of the donor−acceptor systems under investigation here make it important to consider both monomer and dimer chromophores in the computational protocol. We use three cluster models that vary in the size of the QM region and MM region: (i) **M7**: all molecules within **7** Å of a central **monomer** chromophore; (ii) **M15**: all molecules **15** Å from the central **monomer**; and (iii) **D7**: all molecules within **7** Å from a **dimer** chromophore. To simulate the long-range periodic electrostatics, we embed **M15** in Ewald-derived point charges.[48,49] A detailed description of all methods, models, and codes can be found in the Supporting Information.

Our multimodel approach ensures size consistency of the MM region, evaluates the role of short- and long-range interactions, explicitly models the long-range electrostatic potential from the crystal, and determines the role of excitonic coupling and electron transfer on the mechanistic interpretation.

For all models, the crystal environment shifts the bright state to the red with respect to absorption in vacuum. The bright state calculated for **1** with the **M** and **D** models (Table 1) is in very good agreement with the experimental value of 3.3 eV.[41] The bright state is calculated as 2.93 eV with RI-CC2/def2-TZVP. In the case of **2**, the energies predicted with all models are in the range of 3.4 to 3.5 eV, in good agreement with the RI-CC2/def2-TZVP value of 3.33 eV. There is no significant intermolecular charge transfer upon excitation in either material.

The electrostatic potential generated by the whole crystal (in the **Ewald** model) has a negligible effect for the vertical excitations of **1**, with a convergence of 3.3 eV for the bright state. In the case of **2**, a more polar structure, the effect is more significant, with a shift in the energy of ∼0.1 eV. Because this is on the order of the shift associated with vibrations and does not change the nature of the excited states, even the smaller cluster models (**M7** and **D7**) can capture the main electrostatic influence on the photoexcitation.[50]

In going from a monomer chromophore to a dimer chromophore, the bright state shifts from S_1 to S_2 (Supporting Information). For the Franck−Condon (FC) geometry, the electronic density is delocalized over the two chromophores. As a consequence of excitonic coupling, the bright state is blue-shifted in 0.06 and 0.15 eV for **1** and 0.23 and 0.32 eV for **2** (**M7** model as reference). This is typical of H dimers within the Kasha excitonic coupling model, with oscillator strengths of S_2 almost double those of the monomer species in S_1.[51] While the splitting is more significant for **2**, this does not alone explain the different properties of **1** and **2**.

Further understanding can be achieved by calculating the excitonic couplings for the relevant dimers. We apply a diabatization scheme that incorporates both the short-range (exchange, orbital overlap, charge-transfer) and long-range Coulomb interactions.[52] The exciton coupling J between two monomers in a dimer is given in the diabatic 2 × 2 Hamiltonian matrix $\mathbf{H}^D$, computed via

$$\mathbf{H}^D = \mathbf{C}\mathbf{H}^A\mathbf{C}^\dagger \quad (1)$$

Table 1. Absorption Energies from the FC Point and Emission Energies from the E* and K* Minima for QMMM Models[a]

	Compound **1**			Compound **2**		
	Abs. (f)	E* (f)	K* (f)	Abs. (f)	E* (f)	K* (f)
M7	3.20 (1.177)	3.03 (1.207)	2.67 (1.191)	3.42 (0.905)		2.15 (0.461)
M15	3.30 (1.174)	3.10 (1.225)	2.61(0.977)	3.40 (1.005)		2.17 (0.490)
Ewald	3.30 (1.192)	3.12 (1.214)	2.66 (1.052)	3.50 (0.815)		2.18 (0.486)
D7-P	3.26 (2.128)	3.01 (0.479)	2.56 (0.725)	3.51 (1.379)	2.45 (0.002)	2.15 (0.312)
D7-A	3.35 (2.063)	2.96 (0.119)	2.59 (0.616)	3.42 (1.947)	2.81 (0.000)	2.32 (0.388)

[a]Energies are presented in eV and oscillator strengths are given in parentheses, calculated at ONIOM(ωB7X-D/6-311++G(d,p)):AMBER level of theory.

DOI: 10.1021/acs.jpclett.7b02893
J. Phys. Chem. Lett. XXXX, XXX, XXX−XXX

where $\mathbf{H}^A$ is the diagonal Hamiltonian of the S_1 and S_2 excitation energies and **C** is the adiabatic−diabatic transformation matrix. The largest coupling (Table 2) in each

Table 2. *J* Coupling Values (eV) between Units in Dimers of 1 and 2 in the D7 Models

	Compound **1** *J* (eV)	Compound **2** *J* (eV)
D7-P	0.060	0.112
D7-A	0.105	0.150

compound occurs when the monomers are aligned antiparallel (**A**), on the order of 100 meV, which are on the order of those obtained for some organic semiconductors.[53] These couplings result from the favorable alignment between the nitrogen of one monomer and carbonyl group on the other monomer (∼4.5 Å).

Recently, the effect of excitonic couplings on the nonradiative constants for AIE was evaluated.[54] For a set of five highly aromatic conjugated molecules, with *J* values on the order of 10 meV, the authors found that excitonic coupling always increases the nonradiative decay constants. On the basis of these vibronic models, in the E* form, a larger *J* on the nonradiative vibrational decay should be expected for **2**.

Relaxation to either E* or K* minima will follow photoexcitation. Because of the short-range interactions in the dimer models, oscillator strengths for emission are smaller than those obtained for the monomer models (Table 1). In the case of **1**, significant reabsorption is expected due to the small Stokes shift for the E* minimum. This has been recently confirmed experimentally.[55] For **2**, oscillator strengths from E* are extremely small. In this context, no significant emissive response is expected from the E* state of either material. For **1**, relaxation in E* involves localization of the electronic density on one molecule, whereas delocalization is observed for **2**. In vacuum and monomer models, E* is not stable for **2**.

Geometries of the E* and K* minima are planar in the solid state. Because no double proton transfer K* minimum was found for **1**, emission is expected from a localized K* state. The experimental emission spectrum for **1** can be assigned to the K* state ranging from 1.5 to 2.1 eV. The predicted values are blue-shifted to 2.7 eV (CC2/def2-TZVP predicts emission at 2.2 eV). The flatness of the S_1 surface with respect to the dihedral angle suggests that emission from a range of geometries is possible (Supporting Information).

In **2**, there also exists a double-K* state, where both monomers undergo ESIPT. This state is nonemissive in S_1 (f = 0.002), lying 0.5 eV above the bright FC state. The localized single proton transfer state in **2** has emission in the range 2.2 to 2.3 eV (1.7 eV with CC2). Oscillator strengths, though half the value of the obtained for **1**, are still significant (0.312 and 0.388). Although emission from **1** should be brighter than that from 2, radiative mechanisms alone cannot explain the negligible quantum yield of **2**.

The location of the nearest CI to the E* and K* minima can help us to understand the balance between radiative and nonradiative decay. In vacuum, both pathways lead to energetically accessible conical intersections via intramolecular rotation.[56] In the solid, the E* CI is accessed via a stretch of the bridging unsaturated bond, with an energy cost of upward of 5 eV from the FC S_1 energy for both crystals. Consequently, molecular aggregation completely blocks the E* nonradiative decay path.

For **1**, the S_1−S_0 MECI associated with the K* state lies 0.5 to 1.0 eV above the S_1 energy for the FC geometry (Figure 2).

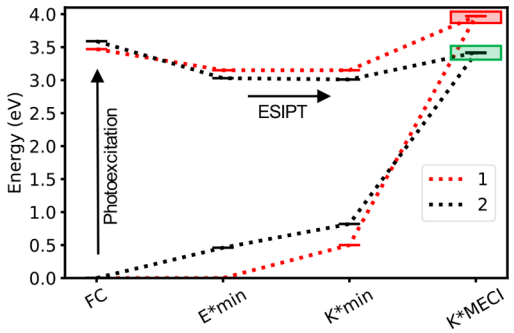

Figure 2. Energy of the S_0 and S_1 states at the Franck−Condon (FC) point, E* and K* minima, and the MECI of **1** and **2** with the **D7** model with ONIOM(ωB7X-D/6-31G(d)):AMBER level of theory. The accessibility is color coded.

For **2**, the S_1−S_0 MECI is classically accessible with a barrier of 0.4 eV from the K* minimum. While less favorable than in the gas phase (barrier 0.2 eV), the system has enough energy provided the initial photoexcitation is to the bright state (S_2). Moreover, within the mechanical embedding approach, the MECI geometries are similar, but both MECI have energies lying above the photopopulated state. This indicates that steric hindrance in the crystal determines the level of distortion of the MECIs, while the Coulombic interactions modulate their total energies.

Crucially, the accessibility of the MECI depends on the stabilization of the MECI with respect the initially populated excited states. For compound **1**, the electrostatic potential stabilizes the S_1 state but has little effect on the energy of the MECI, further decreasing the accessibility of the nonradiative channel (from barrier of 0.2 to 0.6 eV). A similar effect is seen for both the **M7** and **M15** models, suggesting that these are short to medium range effects and are not a result of long-range Coulombic interactions. For **2**, the stabilization of the MECI is larger than for the S_1 state. Therefore, the accessibility of the MECI in **2** is aided by the short-range electrostatic interactions with the surrounding molecules.

The K* MECI is accessed via a combination of intramolecular rotation (ROT) and carbonyl pyramidalization (PYR), with a puckering of the deprotonated phenol ring (Figure 3). These geometries are in good agreement with the obtained with CASSCF (Supporting Information). In contrast with the most stable conical intersections ($\mathbf{CI}_{\mathbf{ROT}}$) in vacuum, the MECI structures in the solid state ($\mathbf{CI}_{\mathbf{PYR}}$) display a significant pyramidalization of the carbonyl carbon and dihedral angles smaller than the 90°. This is essential to minimize the repulsive interactions with the surrounding molecules. For **2**, the K* MECI has similar geometric parameters as **1**, with a smaller pyramidalization of the carbonyl group.

Interestingly, a similar $\mathbf{CI}_{\mathbf{PYR}}$ conical intersection can be found in vacuum (Figure 3), with the $\mathbf{CI}_{\mathbf{PYR}}$ lying 0.9 eV above the $\mathbf{CI}_{\mathbf{ROT}}$ for **1** and 0.6 eV for **2**. Therefore, the crystal changes the order stability of the conical intersection manifold, stabilizing $\mathbf{CI}_{\mathbf{PYR}}$ over $\mathbf{CI}_{\mathbf{ROT}}$ compared with in vacuum. In vacuum, $\mathbf{CI}_{\mathbf{PYR}}$ is energetically accessible once S_1 is populated but for **2** is 0.33 eV below the initial excitation energy. Because the main energetics are already observed in vacuum, the larger stability of the MECI for **2** is mainly explained by the electronic

DOI: 10.1021/acs.jpclett.7b02893
J. Phys. Chem. Lett. XXXX, XXX, XXX−XXX

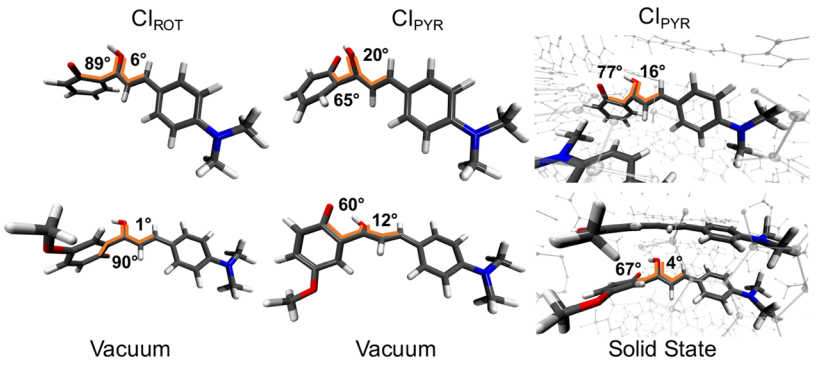

Figure 3. Geometry of the K* MECI in vacuum (left and center) and in the solid state (right). Important geometric parameters are highlighted.

effects provided by the methoxy substituent, aided by the electrostatic potential discussed above. As a result, **2** has enough energy to deactivate through the conical intersection and return to the ground state via the nonradiative pathway, a channel infeasible for compound **1**.

In summary, the analysis of two materials with contrasting emissive properties illustrates how the balance of intermolecular and intramolecular factors can control the radiative and nonradiative mechanisms underlying their light response (Schemes 1 and 2). Considering the radiative mechanisms,

Scheme 1. Mechanism for Nonradiative Decay in Compound 2[a]

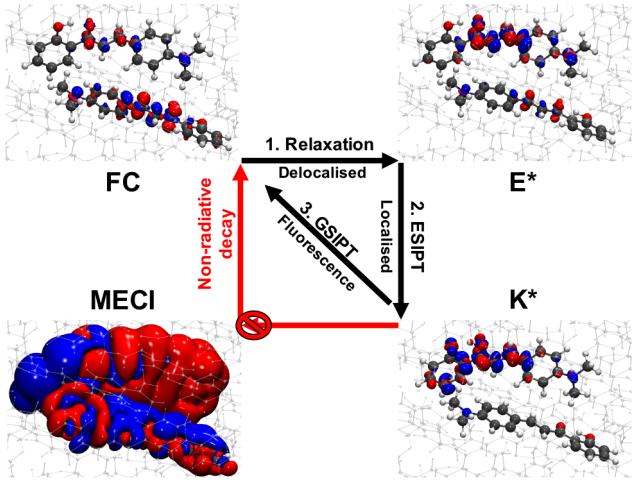

[a]Also shown are S_1-S_0 electron density differences (red: S_1, blue: S_1).

emission from E* is unlikely from the delocalized state in **2** but still possible from K*. The crystal environment also significantly affects the population distribution between of the nonradiative pathways. For both crystals, deactivation through the E* channel is blocked due to a significant increase in the energy of the MECI.

For the K* channel, the crystal changes the relative energy of two conical intersections present in gas phase, stabilizing a structure where the carbonyl group pyramidalizes. While being structurally similar to the MECI of **1**, the MECI of **2** is lower in energy due to the difference in electronic density distribution in S_1 on account of the methoxy group. The $\pi-\pi$ stacking interactions in **2** increase the excitonic coupling. On the contrary, an effective localization of the electronic density is required for the ESIPT process. Our calculations show that either nonradiative delocalized electron-transport processes (E*

Scheme 2. Mechanism for Nonradiative Decay in Compound 2[a]

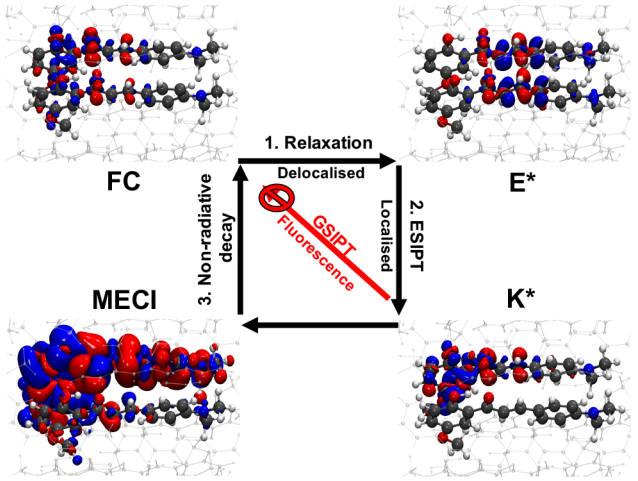

[a]Also shown are S_1-S_0 electron density differences (red: S_1, blue: S_1).

channel) or localized deactivation through the ESIPT (K* channel) are more likely in **2** than in **1**. The interplay of all discussed factors results in an enhance emissive response of **1** and a switch-off of fluorescence in **2** in the solid state.

From our results, some design principles can be proposed for more efficient solid-state emitters. As strong electrostatic interactions aid the deactivation through nonradiative pathways, it is clear why many of the reported AIE fluorophores are nonpolar. For the ESIPT chromophores, stabilizing E* over K* minima could be favorable because the E* nonradiative pathway is hampered in the solid state. For this, the nature of the E* state must be altered to induce a larger Stokes shift. Alternatively, if the E* state is made more unstable by increasing the lability of the transferring proton, then the population of the K* channel will increase. To maximize returns, access to the pyramidal K* MECI can be further hindered by imposing further geometrical restrictions, such as introducing fused rings to the molecular structure. Torsional restraint can also be achieved by coordination to metals.[57] We think that this mechanistic understanding has the potential to contribute to the design of more efficient highly emissive ESIPT materials.

■ ASSOCIATED CONTENT

Supporting Information

The Supporting Information is available free of charge on the ACS Publications website at DOI: 10.1021/acs.jpclett.7b02893.

DOI: 10.1021/acs.jpclett.7b02893
J. Phys. Chem. Lett. XXXX, XXX, XXX−XXX

Computational details, model descriptions, excitation and emission energies, critical point energies, analysis of conical intersections, visualizations of the potential energy surfaces, and crystal structure analysis. (PDF)

AUTHOR INFORMATION

Corresponding Author

*E-mail: r.crespo-otero@qmul.ac.uk.

ORCID

Michael Dommett: 0000-0001-7230-2567

Rachel Crespo-Otero: 0000-0002-8725-5350

Notes

The authors declare no competing financial interest.

ACKNOWLEDGMENTS

This research utilized Queen Mary's Apocrita HPC facility, supported by QMUL Research-IT. We acknowledge the support from the School of Biological and Chemical Sciences at Queen Mary University of London.

REFERENCES

(1) Mei, J.; Leung, N. L. C.; Kwok, R. T. K.; Lam, J. W. Y.; Tang, B. Z. Aggregation-Induced Emission: Together We Shine, United We Soar! *Chem. Rev.* **2015**, *115*, 11718−11940.

(2) Mei, J.; Hong, Y.; Lam, J. W. Y.; Qin, A.; Tang, Y.; Tang, B. Z. Aggregation-Induced Emission: The Whole Is More Brilliant Than the Parts. *Adv. Mater.* **2014**, *26*, 5429−5479.

(3) Hong, Y.; Lam, J. W. Y.; Tang, B. Z. Aggregation-Induced Emission: Phenomenon, Mechanism and Applications. *Chem. Commun.* **2009**, 4332−4335.

(4) Viglianti, L.; Leung, N. L. C.; Xie, N.; Gu, X.; Sung, H. H.-Y.; Miao, Q.; Williams, I. D.; Licandro, E.; Tang, B. Z. Aggregation-Induced Emission: Mechanistic Study of the Clusteroluminescence of Tetrathienylethene. *Chem. Sci.* **2017**, *8*, 2629−2639.

(5) Prlj, A.; Došlić, N.; Corminboeuf, C. How Does Tetraphenylethylene Relax from Its Excited States? *Phys. Chem. Chem. Phys.* **2016**, *18*, 11606−11609.

(6) Gao, Y. J.; Chang, X. P.; Liu, X. Y.; Li, Q. S.; Cui, G.; Thiel, W. Excited-State Decay Paths in Tetraphenylethene Derivatives. *J. Phys. Chem. A* **2017**, *121*, 2572−2579.

(7) Peng, X.-L.; Ruiz-Barragan, S.; Li, Z.-S.; Li, Q.-S.; Blancafort, L. Restricted Access to a Conical Intersection to Explain Aggregation Induced Emission in Dimethyl Tetraphenylsilole. *J. Mater. Chem. C* **2016**, *4*, 2802−2810.

(8) Li, Q.; Blancafort, L. A Conical Intersection Model to Explain Aggregation Induced Emission in Diphenyl Dibenzofulvene. *Chem. Commun.* **2013**, *49*, 5966−5968.

(9) Zhang, C. J.; Feng, G.; Xu, S.; Zhu, Z.; Lu, X.; Wu, J.; Liu, B. Structure-Dependent Cis/Trans Isomerization of Tetraphenylethene Derivatives: Consequences for Aggregation-Induced Emission. *Angew. Chem., Int. Ed.* **2016**, *55*, 6192−6196.

(10) Yang, Z.; Qin, W.; Leung, N. L. C.; Arseneault, M.; Lam, J. W. Y.; Liang, G.; Sung, H. H. Y.; Williams, D.; Tang, B. Z. A Mechanistic Study of AIE Processes of TPE Luminogens: Intramolecular Rotation vs. Configurational Isomerization. *J. Mater. Chem. C* **2016**, *4*, 99−107.

(11) Rao M, R.; Liao, C.-W.; Su, W.-L.; Sun, S.-S. Quinoxaline Based D-A-D Molecules: High Contrast Reversible Solid-State Mechano- And Thermo-Responsive Fluorescent Materials. *J. Mater. Chem. C* **2013**, *1*, 5491−5501.

(12) Cai, M.; Gao, Z.; Zhou, X.; Wang, X.; Chen, S.; Zhao, Y.; Qian, Y.; Shi, N.; Mi, B.; Xie, L.; et al. A Small Change in Molecular Structure, a Big Difference in the AIEE Mechanism. *Phys. Chem. Chem. Phys.* **2012**, *14*, 5289−5296.

(13) Du, X.; Qi, J.; Zhang, Z.; Ma, D.; Wang, Z. Y. Efficient Non-Doped Near Infrared Organic Light-Emitting Devices Based on Fluorophores with Aggregation-Induced Emission Enhancement. *Chem. Mater.* **2012**, *24*, 2178−2185.

(14) Peng, Q.; Yi, Y.; Shuai, Z.; Shao, J. Toward Quantitative Prediction of Molecular Fluorescence Quantum Efficiency: Role of Duschinsky Rotation. *J. Am. Chem. Soc.* **2007**, *129*, 9333−9339.

(15) Peng, Q.; Yi, Y.; Shuai, Z.; Shao, J. Excited State Radiationless Decay Process with Duschinsky Rotation Effect: Formalism and Implementation. *J. Chem. Phys.* **2007**, *126*, 114302−114309.

(16) Yin, S.; Peng, Q.; Shuai, Z.; Fang, W.; Wang, Y. H.; Luo, Y. Aggregation-Enhanced Luminescence and Vibronic Coupling of Silole Molecules from First Principles. *Phys. Rev. B: Condens. Matter Mater. Phys.* **2006**, *73*, 1−5.

(17) Duan, Y. C.; Wu, Y.; Jin, J. L.; Gu, D. M.; Geng, Y.; Zhang, M.; Su, Z. M. Influence of Aggregation on the Structure and Fluorescent Properties of a Tetraphenylethylene Derivative: A Theoretical Study. *ChemPhysChem* **2017**, *18*, 755−762.

(18) Lin, L.; Fan, J.; Cai, L.; Wang, C.-K. Theoretical Perspective of the Excited State Intramolecular Proton Transfer for a Compound with Aggregation Induced Emission in the Solid Phase. *RSC Adv.* **2017**, *7*, 44089−44096.

(19) Fan, J.; Lin, L.; Wang, C.-K. Excited State Properties of Non-Doped Thermally Activated Delayed Fluorescence Emitters with Aggregation-Induced Emission: A QM/MM Study. *J. Mater. Chem. C* **2017**, *5*, 8390−8399.

(20) Presti, D.; Pedone, A.; Ciofini, I.; Labat, F.; Menziani, M. C.; Adamo, C. Optical Properties of the Dibenzothiazolylphenol Molecular Crystals Through ONIOM Calculations: The Effect of the Electrostatic Embedding Scheme. *Theor. Chem. Acc.* **2016**, *135*, 1−11.

(21) Fan, J.; Cai, L.; Lin, L.; Wang, C.-K. Dynamics of Excited States for Fluorescent Emitters with Hybridized Local and Charge-Transfer Excited State in Solid Phase: A QM/MM Study. *J. Phys. Chem. A* **2016**, *120*, 9422−9430.

(22) Wang, B.; Wang, X.; Wang, W.; Liu, F. Exploring the Mechanism of Fluorescence Quenching and Aggregation-Induced Emission of a Phenylethylene Derivative by QM (CASSCF and TDDFT) and ONIOM (QM:MM) Calculations. *J. Phys. Chem. C* **2016**, *120*, 21850−21857.

(23) Zhang, T.; Ma, H.; Niu, Y.; Li, W.; Wang, D.; Peng, Q.; Shuai, Z.; Liang, W. Z. Spectroscopic Signature of the Aggregation-Induced Emission Phenomena Caused by Restricted Nonradiative Decay: A Theoretical Proposal. *J. Phys. Chem. C* **2015**, *119*, 5040−5047.

(24) Wu, Q.; Zhang, T.; Peng, Q.; Wang, D.; Shuai, Z. Aggregation Induced Blue-Shifted Emission - The Molecular Picture from a QM/MM Study. *Phys. Chem. Chem. Phys.* **2014**, *16*, 5545−5552.

(25) Wu, Q.; Peng, Q.; Niu, Y.; Gao, X.; Shuai, Z. Theoretical Insights Into the Aggregation-Induced Emission by Hydrogen Bonding: A QM/MM Study. *J. Phys. Chem. A* **2012**, *116*, 3881−3888.

(26) Li, M.-C.; Hayashi, M.; Lin, S.-H. Quantum Chemistry Study on Internal Conversion of Diphenyldibenzofulvene in Solid Phase. *J. Phys. Chem. A* **2011**, *115*, 14531−14538.

(27) Padalkar, V. S.; Seki, S. Excited-State Intramolecular Proton-Transfer (ESIPT)-inspired Solid State Emitters. *Chem. Soc. Rev.* **2016**, *45*, 169−202.

(28) Zhao, J.; Ji, S.; Chen, Y.; Guo, H.; Yang, P. Excited State Intramolecular Proton Transfer (ESIPT): from Principal Photophysics to the Development of New Chromophores and Applications in Fluorescent Molecular Probes and Luminescent Materials. *Phys. Chem. Chem. Phys.* **2012**, *14*, 8803−8817.

(29) Kwon, J. E.; Park, S. Y. Advanced Organic Optoelectronic Materials: Harnessing Excited-State Intramolecular Proton Transfer (ESIPT) Process. *Adv. Mater.* **2011**, *23*, 3615−3642.

(30) Hsieh, C.-C.; Jiang, C.-M.; Chou, P.-T. Recent Experimental Advances on Excited-State Intramolecular Proton Coupled Electron Transfer Reaction. *Acc. Chem. Res.* **2010**, *43*, 1364−1374.

(31) Azarias, C.; Budzák, Š.; Laurent, A. D.; Ulrich, G.; Jacquemin, D. Tuning ESIPT Fluorophores Into Dual Emitters. *Chem. Sci.* **2016**, *7*, 3763−3774.

DOI: 10.1021/acs.jpclett.7b02893
J. Phys. Chem. Lett. XXXX, XXX, XXX−XXX

(32) Ghosh, D.; Ahamed, G.; Batuta, S.; Begum, N. A.; Mandal, D. Effect of an Electron-Donating Substituent at the 3′,4′-Position of 3-Hydroxyflavone: Photophysics in Bulk Solvents. *J. Phys. Chem. A* **2016**, *120*, 44−54.
(33) Cheng, J.; Liu, D.; Li, W.; Bao, L.; Han, K. Comprehensive Studies on Excited-State Proton Transfer of a Series of 2-(2′-Hydroxyphenyl)benzothiazole Derivatives: Synthesis, Optical Properties, and Theoretical Calculations. *J. Phys. Chem. C* **2015**, *119*, 4242−4251.
(34) Baker, L. a.; Horbury, M. D.; Greenough, S. E.; Coulter, P. M.; Karsili, T. N. V.; Roberts, G. M.; Orr-Ewing, A. J.; Ashfold, M. N. R.; Stavros, V. G. Probing the Ultrafast Energy Dissipation Mechanism of the Sunscreen Oxybenzone After UVA Irradiation. *J. Phys. Chem. Lett.* **2015**, *6*, 1363−1368.
(35) Wilbraham, L.; Savarese, M.; Rega, N.; Adamo, C.; Ciofini, I. Describing Excited State Intramolecular Proton Transfer in Dual Emissive Systems: A Density Functional Theory Based Analysis. *J. Phys. Chem. B* **2015**, *119*, 2459−2466.
(36) Demchenko, A. P.; Tang, K.-C.; Chou, P.-T. Excited-State Proton Coupled Charge Transfer Modulated by Molecular Structure and Media Polarization. *Chem. Soc. Rev.* **2013**, *42*, 1379−1408.
(37) Barbatti, M.; Aquino, A. J. a.; Lischka, H.; Schriever, C.; Lochbrunner, S.; Riedle, E. Ultrafast Internal Conversion Pathway and Mechanism in 2-(2′-Hydroxyphenyl)benzothiazole: A Case Study for Excited-State Intramolecular Proton Transfer Systems. *Phys. Chem. Chem. Phys.* **2009**, *11*, 1406−1415.
(38) Yushchenko, D. a.; Shvadchak, V. V.; Klymchenko, A. S.; Duportail, G.; Pivovarenko, V. G.; Mély, Y. Modulation of Excited-State Intramolecular Proton Transfer by Viscosity in Protic Media. *J. Phys. Chem. A* **2007**, *111*, 10435−10438.
(39) Klymchenko, A. S.; Demchenko, A. P. Multiparametric Probing of Intermolecular Interactions with Fluorescent Dye Exhibiting Excited State Intramolecular Proton Transfer. *Phys. Chem. Chem. Phys.* **2003**, *5*, 461−468.
(40) Crespo-Otero, R.; Mardykov, A.; Sanchez-Garcia, E.; Sander, W.; Barbatti, M. Photo-Stability of Peptide-Bond Aggregates: N-Methylformamide Dimers. *Phys. Chem. Chem. Phys.* **2014**, *16*, 18877−18887.
(41) Cheng, X.; Wang, K.; Huang, S.; Zhang, H.; Zhang, H.; Wang, Y. Organic Crystals with Near-Infrared Amplified Spontaneous Emissions Based on 2′-Hydroxychalcone Derivatives: Subtle Structure Modification but Great Property Change. *Angew. Chem., Int. Ed.* **2015**, *54*, 8369−8373.
(42) Giannozzi, P.; Baroni, S.; Bonini, N.; Calandra, M.; Car, R.; Cavazzoni, C.; Ceresoli, D.; Chiarotti, G. L.; Cococcioni, M.; Dabo, I.; et al. QUANTUM ESPRESSO: A Modular and Open-Source Software Project for Quantum Simulations of Materials. *J. Phys.: Condens. Matter* **2009**, *21*, 395502.
(43) Dapprich, S.; Komaromi, I.; Byun, K. S.; Morokuma, K.; Frisch, M. J. A New ONIOM Implementation in Gaussian98. Part I. The Calculation of Energies, Gradients, Vibrational Frequencies and Electric Field Derivatives. *J. Mol. Struct.: THEOCHEM* **1999**, *462*, 1−21.
(44) Vreven, T.; Morokuma, K.; Farkas, Ö.; Schlegel, H. B.; Frisch, M. J. Geometry Optimization with QM/MM, ONIOM, and Other Combined Methods. I. Microiterations. *J. Comput. Chem.* **2003**, *24*, 760−769.
(45) Chung, L. W.; Sameera, W. M. C.; Ramozzi, R.; Page, A. J.; Hatanaka, M.; Petrova, G. P.; Harris, T. V.; Li, X.; Ke, Z.; Liu, F.; et al. The ONIOM Method and Its Applications. *Chem. Rev.* **2015**, *115*, 5678−5796.
(46) Levine, B. G.; Coe, J. D.; Martínez, T. J. Optimizing Conical Intersections Without Derivative Coupling Vectors: Application to Multistate Multireference Second-Order Perturbation Theory (MS-CASPT2). *J. Phys. Chem. B* **2008**, *112*, 405−413.
(47) Crespo-Otero, R.; Kungwan, N.; Barbatti, M. Stepwise Double Excited-State Proton Transfer Is Not Possible in 7-Azaindole Dimer. *Chem. Sci.* **2015**, *6*, 5762−5767.
(48) Klintenberg, M.; Derenzo, S. E.; Weber, M. J. Accurate Crystal Fields for Embedded Cluster Calculations. *Comput. Phys. Commun.* **2000**, *131*, 120−128.
(49) Derenzo, S. E.; Klintenberg, M. K.; Weber, M. J. Determining Point Charge Arrays That Produce Accurate Ionic Crystal Fields for Atomic Cluster Calculations. *J. Chem. Phys.* **2000**, *112*, 2074−2081.
(50) Crespo-Otero, R.; Barbatti, M. Spectrum Simulation and Decomposition with Nuclear Ensemble: Formal Derivation and Application to Benzene, Furan and 2-Phenylfuran. *Theor. Chem. Acc.* **2012**, *131*, 1−14.
(51) Kasha, M.; Rawls, H. R.; Ashraf El-Bayoumi, M. The Exciton Model in Molecular Spectroscopy. *Pure Appl. Chem.* **1965**, *11*, 371−392.
(52) Aragó, J.; Troisi, A. Dynamics of the Excitonic Coupling in Organic Crystals. *Phys. Rev. Lett.* **2015**, *114*, 1−5.
(53) Fornari, R. P.; Rowe, P.; Padula, D.; Troisi, A. Importance and Nature of Short-Range Excitonic Interactions in Light Harvesting Complexes and Organic Semiconductors. *J. Chem. Theory Comput.* **2017**, *13*, 3754−3763.
(54) Li, W.; Zhu, L.; Shi, Q.; Ren, J.; Peng, Q.; Shuai, Z. Excitonic Coupling Effect on the Nonradiative Decay Rate in Molecular Aggregates: Formalism and Application. *Chem. Phys. Lett.* **2017**, *683*, 507−514.
(55) Zahid, N. I.; Mahmood, M. S.; Subramanian, B.; Mohd Said, S.; Abou-Zied, O. K. New Insight into the Origin of the Red/Near-Infrared Intense Fluorescence of a Crystalline 2-Hydroxychalcone Derivative: A Comprehensive Picture from the Excited-State Femtosecond Dynamics. *J. Phys. Chem. Lett.* **2017**, *8*, 5603−5608. PMID: 29094952.
(56) Dommett, M.; Crespo-Otero, R. Excited State Proton Transfer in 2′-Hydroxychalcone Derivatives. *Phys. Chem. Chem. Phys.* **2017**, *19*, 2409−2416.
(57) Karsili, T. N. V.; Marchetti, B.; Ashfold, M. N. R. Mechanistic Insights Into Excited State Intramolecular Proton Transfer in Isolated and Metal Chelated Supramolecular Chemosensors. *Dalt. Trans.* **2016**, *45*, 18921−18930.

DOI: 10.1021/acs.jpclett.7b02893
J. Phys. Chem. Lett. XXXX, XXX, XXX−XXX